Published in final edited form as:
Cancer Res. 2009 March 15; 69(6): 2201–2209. doi:10.1158/0008-5472.CAN-08-1301.

ADP-Ribosylation Factor 6 Regulates Tumorigenic and Invasive Properties *In vivo*

Vandhana Muralidharan-Chari[1], **Holly Hoover**[1], **James Clancy**[1], **Jill Schweitzer**[1], **Mark A. Suckow**[1,2], **Valerie Schroeder**[2], **Francis J. Castellino**[3], **Jeffrey S. Schorey**[1], and **Crislyn D'Souza-Schorey**[1]

[1]Department of Biological Sciences, University of Notre Dame, Notre Dame, Indiana

[2]Freimann Life Science Center, University of Notre Dame, Notre Dame, Indiana

[3]W.M. Keck Center for Transgene Research, University of Notre Dame, Notre Dame, Indiana

Abstract

This study shows that the small GTP-binding protein ADP-ribosylation factor 6 (ARF6) is an important regulator of tumor growth and metastasis. Using spontaneous melanoma tumor growth assays and experimental metastasis assays in nude mice, we show that sustained activation of ARF6 reduces tumor mass growth but significantly enhances the invasive capacity of tumor cells. In contrast, mice injected with tumor cells expressing a dominantly inhibitory ARF6 mutant exhibited a lower incidence and degree of invasion and lung metastasis compared with control animals. Effects on tumor growth correlate with reduced cell proliferation capacity and are linked at least in part to alterations in mitotic progression induced by defective ARF6 cycling. Furthermore, phospho-ERK levels in subcultured cells from ARF6(GTP) and ARF6(GDP) tumor explants correlate with invasive capacity. ARF6-induced extracellular signal-regulated kinase (ERK) signaling leads to Rac1 activation to promote invadopodia formation and cell invasion. These findings document an intricate role for ARF6 and the regulation of ERK activation in orchestrating mechanisms underlying melanoma growth, invasion, and metastases.

Introduction

Metastasis is a complex and multistep process that depends on the ability of tumor cells to successfully break away from the primary tumor and colonize at distant sites. When tumor cells detach from the primary tumor, they "invade" surrounding tissues and the host circulation, followed by extravasation into distant organs (1). Increased signaling, cytoskeletal rearrangements, and the directed targeting of matrix proteases to the extracellular space, all accompany the process of tumor cell invasion (2, 3).

Requests for reprints: Crislyn D'Souza-Schorey, Department of Biological Sciences, University of Notre Dame, Box 369, Galvin Life Sciences Building, Notre Dame, IN 46556-0369. Phone: 574-631-3735; Fax: 574-631-7413; D'Souza-Schorey.1@nd.edu or cdsouzas@nd.edu.
V. Muralidharan-Chari and H. Hoover contributed equally to this work.

Note: Supplementary data for this article are available at Cancer Research Online (http://cancerres.aacrjournals.org/).

Note Added in Proof
Since this article was accepted, Hu et al. reported that ARF6 regulates glioma cell invasion via a Rac1-dependent pathway. (Cancer Research 2009;69:794–801).

Disclosure of Potential Conflicts of Interest
No potential conflicts of interest were disclosed.

ADP-ribosylation factor 6 (ARF6) is a member of the ARF family of the Ras superfamily of small GTPases that alternates in cells between its active GTP-bound and an inactive GDP-bound forms. Over the past few years, ARF6, via its well-established roles in the regulation of endosomal membrane trafficking and actin cytoskeleton remodeling, has been shown to regulate acquisition of migratory potential in a variety of cell types (4, 5). Indeed, by directing specific cargo to discrete sites at the cell surface and/or promoting the formation of surface protrusions, ARF6 has been shown to regulate phagocytosis, intercellular adhesion, and, pertinent to this study, tumor cell invasion (reviewed in ref. 5). Recent studies using *in vitro* cell invasion assays have indicated that in invasive melanoma, glioma, and breast cancer cell lines, the ARF6 GTPase cycle can regulate invasive potential (6–8). These studies have shown that depletion of cellular levels of ARF6 by siRNA or expression of dominant-negative ARF6 mutants, blocks tumor cell invasion, and degradation of surrounding extracellular matrix proteins (6, 7). It has also been documented that endogenous levels of active ARF6-GTP increases in response to physiologic agonists that stimulate cell invasion (6). Furthermore, screening of various breast tumor cell lines has revealed a direct correlation between ARF6 protein expression and tumor invasive capacity (7). Finally, in melanoma and glioma cell lines, ARF6-GTP has been shown to promote cell invasion at least in part by activating the extracellular signal-regulated kinase (ERK; refs. 6, 8).

The goal of this study was to examine the role of ARF6 in tumor cell invasion *in vivo*. Using the invasive melanoma cell line, LOX, and athymic nude mice as a model system, we have investigated the role of ARF6 in invasion and metastases by examining the effects of ARF6 mutants defective in GTP/GDP cycling. We find that the constitutive activation of ARF6 reduces tumor mass growth but significantly enhances the invasive capacity of tumor cells. Dominant inhibition of ARF6 function delays the rate of tumor growth as well as local invasion and metastases. The effects on tumor growth are linked at least in part with alterations in mitotic progression induced by defective ARF6 cycling. ARF6-regulated cell invasion is dependent on ERK and Rac1 activation. The findings described here document an important role for ARF6 in modulating tumor growth and invasion *in vivo* and underscore the importance of ERK activation in cell invasion, downstream of ARF6.

Materials and Methods

Plasmids

Generation of plasmids, pTRE2-ARF6(Q67L)-HA, and pTRE2-ARF6(T27N)-HA is described in Supplementary Information. Plasmids encoding green fluorescent protein–phosphatidic acid (GFP-PABD) binding domain (9) was kindly provided by Dr. Nicholas Vitale (Centre National de la Recherche Scientifique & Universite Louis Pasteur, Strasbourg, France). Plasmids encoding Rac1(T17N) and HA-ARF6(Q67L) have been described (10).

Cell culture and transfection

LOX cell lines were cultured as previously described (6). The method for generation of stable cell lines expressing ARF6-GTP/GDP mutants is described in the Supplementary Information.

Immunofluorescent staining and microscopy

LOX cells were cultured on glass coverslips, fixed, and processed as described (6, 11). Fluorescence was visualized using a Bio-Rad or Leica laser confocal scanning system.

Cell proliferation assays

Cell proliferation was monitored by crystal violet staining as previously described (12). Additional cell proliferation assays and doubling time measurements are described in Supplementary Information.

In vivo tumorigenicity and metastasis assays

Five-week-old athymic, male mice (NIH) were maintained under environmental conditions as described in the NIH *Guide for the Care and Use of Laboratory Animals* (see Supplementary Information). For s.c. tumor growth experiments, mice were injected s.c. in the lumbar-dorsal region with 1×10^6 LOX cells in 0.1 mL injection medium. Mice were maintained on an irradiated, nutritionally adequate (doxycyline-free) diet. Tumor volumes were calculated according to the formula (volume = $0.52 \times \text{width}^2 \times \text{length}$) for estimating the volume of an ellipsoid. Mice were sacrificed up to 6 wk later or when animals displayed clinical signs suggestive of significant tumor burden. For experimental lung metastasis assays, animals were injected i.v. with 1×10^6 LOX cells in 0.2 mL injection medium via the lateral tail veins. Experiments were performed as two or three independent rounds of injections.

Histology methods

Mice were anesthetized, perfused with fixative, and processed for histology as previously described (13). Standard H&E and Masson's Trichrome staining procedures were used to observe histopathologic characteristics. Tissue sections expressing GFP were labeled with ToPro-3, a nuclear stain. For quantitation of metastases, the percentage of tumor tissue to total lung tissue was calculated using Image J software.[4]

In vitro cell invasion assay

The cell invasion assay was performed as previously described (6, 11). Briefly, cells were seeded on fluorescent gelatincoated coverslips. For quantitation of cell invasion, at least 120 cells were visualized for each experimental condition and those exhibiting gelatin degradation underneath were scored. The percentage of cells degrading gelatin was calculated as an indicator of cell invasion.

Tumor explant subculture

Tumors from lungs and other tissues were harvested and isolated as described (14). Cell suspensions were plated in medium containing G418 for selection of LOX^{GFP} cells.

ARF6-GTP pull-down assay

Levels of ARF6-GTP were measured using a pull-down assay as previously described (15).

Western blot analysis and antibodies

Standard protocols were used. Antibodies used are anti-GFP (Roche), mouse anti-HA (Covance), mouse anti-Myc antibody, Clone 9B11 (Cell Signaling Technologies), anti-mouse monoclonal phospho-p44/42 ERK, E10 (Cell Signaling Technologies), antirabbit polyclonal p44/42 antibody (Cell Signaling Technologies), and anti-a-tubulin (Sigma).

[4] http://rsb.info.nih.gov/ij/

Cell cycle analyses and mitotic synchronization

To analyze progression through cytokinesis, mitotic LOX cells were synchronized as previously described (15) and analyzed using immunofluorescence microscopy post entry into mitosis. Flow cytometry was performed using a Cytomics FC-500 flow cytometer (Beckman Coulter) and the percentage of cells undergoing apoptosis in each phase of the cell cycle phase was determined according to an internal protocol.

Results

Characterization of LOX cells expressing ARF6 GTP/GDP cycling-defective mutants

LOX is a highly invasive melanoma cell line. For these investigations, we generated clonal populations of LOX cell lines capable of stable expression of hemagglutinin (HA)-tagged constitutively activated]GTP-bound, and dominantnegative GDP-bound ARF6 mutants, ARF6(Q67L)-HA, and ARF6(T27N)-HA, respectively, as well as GFP. Western analysis was performed on all Tet-Off clones surviving selection to confirm transgene expression (Supplementary Fig. S1*A*). In addition, lysates were subjected to an ARF6-GTP pull-down assay (15). As expected, lysates from the ARF6(Q67L) stable LOX cells exhibited a high level of ARF6-GTP compared with the parental and ARF6(T27N)-LOX cells (Supplementary Fig. S1*B*). Endogenous ARF6 levels were similar in parental, stable GFP, and mutant ARF6-LOX cell lines. Immunofluorescent staining showed that consistent with previous observations (6), ARF6(GDP) is predominantly localized to the perinuclear cytoplasm, whereas ARF6(GTP) is predominantly localized to the cell surface of $LOX^{ARF6\text{-}GDP}$ and $LOX^{ARF6\text{-}GTP}$ cells, respectively (Supplementary Fig. S1*C*). Cell lines expressing GFP, ARF6(Q67L), and ARF6(T27N) will henceforth be called LOX^{GFP}, $LOX^{ARF6\text{-}GTP}$, and $LOX^{ARF6\text{-}GDP}$, respectively.

The ARF6 GTP/GDP cycle regulates tumor growth

LOX^{GFP}, $LOX^{ARF6\text{-}GTP}$, and $LOX^{ARF6\text{-}GDP}$ cells were injected s.c. into the flanks of 5-week-old athymic, male mice. All cells lines injected formed palpable tumors by 1 week. Primary tumors formed from LOX^{GFP} cells had a steady growth rate over time. These mice formed large s.c. tumors and were sacrificed at early time points to minimize tumor burden in accordance with animal care guidelines. Tumors formed by $LOX^{ARF6\text{-}GDP}$ cells also grew steadily, albeit not to the same degree and at a slower rate relative to LOX^{GFP} control tumors (Fig. 1*A* and *B*). In marked contrast, however, primary tumors formed by $LOX^{ARF6\text{-}GTP}$ cells remained notably small.

To confirm that alterations in tumor volume were direct effects of expressing ARF6 mutants, we analyzed the growth rate of the LOX^{GFP}, $LOX^{ARF6\text{-}GTP}$, and $LOX^{ARF6\text{-}GDP}$ cells using *in vitro* proliferation assays. LOX cells were plated and counted (Supplementary Fig. S2*A*), or stained with crystal violet over a period of 4 days (Fig. 1*C*). As shown, $LOX^{ARF6\text{-}GDP}$ cells grew slightly slower with doubling time of 24.8 ± 0.9 hours, compared with 22.4 ± 2.1 hours in parental LOX^{GFP} cells. However, the $LOX^{ARF6\text{-}GTP}$ cell line grew at a significantly reduced rate with a doubling time of 34.2 ± 1.4 hours. We also assessed the relative levels of Myc in each of the stable cell lines. Myc coordinates gene expression involved in cell cycle progression and contributes to tumorigenesis by inducing unrestrained cellular growth and proliferation (16). We found that the levels of Myc were similar in LOX^{GFP} and $LOX^{ARF6\text{-}GDP}$ cells but dramatically decreased in $LOX^{ARF6\text{-}GTP}$ cells, as measured by Western analysis (Fig. 1*D*). We performed cell cycle analysis on the LOX lines (Fig. 2*A*) and cells obtained from the primary tumor (Supplementary Table S1). Although there is no block during progression through the cell cycle, there is a small increase in the number of cells in the G_2-M phase with expression of the ARF6-GDP mutant. However, we find a more pronounced increase in $LOX^{ARF6\text{-}GTP}$ cells in G_2-M along with a significant

decrease in the number of cells in the S phase. Also, there are no major alterations in the cells undergoing apoptosis. To further confirm that the reduced growth rate of the $LOX^{ARF6\text{-}GTP}$ stable line was due to a decrease in proliferation and not cell death, lactate dehydrogenase (LDH) release was measured (data not shown). After 4 days of culture, LDH levels remained similarly low in all cell lines tested, suggesting that the decreased proliferation rate in $LOX^{ARF6\text{-}GTP}$ cells is not due to an increase in cell death (data not shown).

Constitutive activation of ARF6 in cell culture results in a significant delay in the completion of cytokinesis, the terminal stage of mitosis (11, 17). To determine whether the decrease in tumor growth in $LOX^{ARF6\text{-}GTP}$ cells correlates with changes in cytokinesis, cells subcultured from $LOX^{ARF6\text{-}GTP}$ tumors were examined for progression through mitosis. Cells were synchronized using double-thymidine block followed by nocodazole arrest. Although all the synchronized cells reached late telophase/early cytokinesis by 90 minutes after entry into mitosis, $LOX^{ARF6\text{-}GTP}$ cells frequently remained connected by thin tubulin-positive intercellular bridges at 4 to 5 hours after mitotic entry (Fig. 2*B*).

Although only 3.7% of parental LOX cells exhibited this phenotype, ~3- to 6-fold more $LOX^{ARF6\text{-}GTP}$ cells, either the parental cell line or those derived from the primary tumor, were still connected. Thus, the decrease in cell proliferation leading to reduced tumor growth is due at least in part to aberrant effects of ARF6-GTP on the cell division machinery.

Effect of ARF6 on primary tumor invasion

In addition to tumor growth, we also monitored the invasive capabilities of the primary tumors formed by LOX^{GFP}, $LOX^{ARF6\text{-}GTP}$, and $LOX^{ARF6\text{-}GDP}$ cells. S.c. injections of melanoma as described above allows cell invasion through the subcutaneous muscle, fat, and dermal layers (reverse metastases); therefore, examination of the tumor-skin interface serves as a good indicator of localized invasion. Thus, serial sections from tumors at the tumor-skin interface were analyzed for GFP or stained with Masson's Trichrome. Supplementary Fig. S3*A* and *B* show the progression of LOX^{GFP} invasion with time. At 3 weeks postinjection, these cells showed a high degree of cell invasion, as measured by the extent of collagen border compromise and infiltration into surrounding muscle and skin. Expression of ARF6 GTP/GDP mutants significantly affected the kinetics of LOX invasion. Approximate time-matched $LOX^{ARF6\text{-}GDP}$ tumors displayed cell invasion, although to a much reduced extent relative to LOX^{GFP} because in some areas, the tumor border at the tumor-skin interface remained largely intact and did not display evidence of invasion (Fig. 3). Time-matched $LOX^{ARF6\text{-}GTP}$ tumors on the other hand, although four to five times smaller than the LOX^{GFP} tumors, were significantly more invasive (Fig. 3). Large areas of the collagen border and muscle tissue surrounding the primary tumor mass were completely obliterated and replaced by ARF6-GTP–expressing tumor cells. When size-matched LOX^{GFP} and $LOX^{ARF6\text{-}GTP}$ tumors were compared, the effect of sustained ARF6 activation on invasion potential is even more pronounced (Fig. 4*A*–*C*). Although the border of relatively small LOX^{GFP} tumors measuring ~400 mm^3 is intact, ARF6-GTP– expressing tumors in the same size range showed compromise to the tumor border at the tumor-skin interface and localized invasion into surrounding fat tissue. In a second set of size-matched experiments, $LOX^{ARF6\text{-}GTP}$ primary tumors were allowed to grow for ~57 days to enlarge their masses to a size comparable with that of invasive LOX^{GFP} tumors (~4,000 mm^3). These larger primary ARF6-GTP tumors invaded far into the epidermis and the collagen border, muscle cells, and subcutaneous fat layers were markedly compromised (Fig. 4*D*–*F*). This was significantly more invasive than that observed for size-matched LOX^{GFP} tumors.

Figure 4*G* to *H* compares sections of LOX^{GFP} and $LOX^{ARF6\text{-}GTP}$ tumors demonstrating a similar degree of invasion into surrounding tissues. The collagen and muscle layers exhibit a comparable extent of compromise. Of note is that the $LOX^{ARF6\text{-}GTP}$ tumor shown is 25% the size of the LOX^{GFP} tumor. Collectively, these findings indicate that although sustained ARF6 activation reduces tumor mass growth, it confers significant invasive potential to cells of the primary tumor.

Effect of ARF6 on experimental lung metastasis

Studies with metastasis models of athymic nude mice have shown that LOX cells have a preference for growth in the lungs (18, 19). However, reverse metastases often decreases the efficiency at which these melanoma cells reach the lung. Therefore, in addition to the spontaneous metastasis model, an experimental metastasis assay that has been used extensively to study the events that occur after intravasation (14, 18) was used to observe the effects of ARF6 on metastatic behavior *in vivo*. For these latter studies, 1×10^6 cells were injected into the tail vein and mice were observed on a regular basis for respiratory dyspnea, and time-matched sets of mice were sacrificed when signs of distress were apparent. Gross pathologic examination of lungs showed that mice injected with LOX^{GFP} cells had the greatest extent of metastatic burden. These mice sacrificed at 43 or 53 days postinjection displayed numerous macrometastatic lesions (Fig. 5*A*). Mice injected with LOX cells displayed a moderate degree of metastatic burden at the same postinjection times, and lungs from these mice had fewer and smaller macrometastatic lesions compared with lungs from LOX^{GFP} -injected mice (Fig. 5*A*). Furthermore, the incidence of lung metastases was 43% relative to 67% in LOX^{GFP} -injected mice. We also observed metastatic lesions in the lymph nodes, soft tissues associated with stifle joint and testicular tissues. In stark contrast, lungs from mice injected with $LOX^{ARF6\text{-}GTP}$cells did not show any visible macroscopic metastases even at longer postinjection times (Fig. 5*A*).

Lungs were also examined for micrometastases. In accord with gross examination, lungs from mice injected with LOX cells showed the greatest degree of tumor burden where much of the lung tissue was replaced by tumor cells (Fig. 5*B*). Lungs excised from mice injected with $LOX^{ARF6\text{-}GDP}$ cells showed several small tumors in most of the lobes (Fig. 5*B*). However, the lungs obtained from mice injected with $LOX^{ARF6\text{-}GTP}$ cells exhibited only microscopic metastases that were not detectable by gross examination (Fig. 5*B*, *far right column*). Thus, sustained activation of ARF6, such as its effect on primary tumor growth, dramatically reduces the efficiency of macrometastases formation.

In our previous investigations, we showed that expression of dominant-negative ARF6-GDP in LOX cells abolished invadopodia formation and, hence, cell invasion in *in vitro* assays for cell invasion (6). Given the findings described here, we examined the ability of metastasized $LOX^{ARF6\text{-}GDP}$ cells to form invadopodia. To this end, we generated several subcultures from LOX^{GFP} and $LOX^{ARF6\text{-}GDP}$ macrometastases in lung, lymph nodes, and testis, resulting from lateral tail vein injections. Representative fluorescence and phase contrast images of the LOX^{GFP} and $LOX^{ARF6\text{-}GDP}$ subcultured cells are shown in Supplementary Fig. S4. We were unable to generate subcultures from the $LOX^{ARF6\text{-}GTP}$ lung microlesions, likely due to their reduced capacity to proliferate in addition to limited cell numbers. As seen in Fig. 5*C*, when seeded on gelatin-coated coverslips and labeled for cortactin, a bone fide component of invadopodia, unlike the parental $LOX^{ARF6\text{-}GDP}$ cell line, $LOX^{ARF6\text{-}GDP}$ cells subcultured from tumor explants exhibit prominent invadopodia, suggesting that compensatory pathways in tumors come into play to rescue invasiveness.

ERK activation in metastatic tumor explants

Previous studies also showed that ARF6-regulated invasion was dependent on ERK activity (6, 8). ARF6-GTP facilitated ERK activation, whereas ARF6-GDP–expressing cells exhibited significantly lower levels of activated ERK relative to invasive LOX cells. Thus, we examined the levels of phospho-ERK levels in $LOX^{ARF6\text{-}GDP}$ cells subcultured from tumor explants compared with their parental counterparts. However, phospho-ERK levels in the $LOX^{ARF6\text{-}GDP}$ subcultured cell lines are higher than the parental line (Fig. 5*D*). These findings suggest that the $LOX^{ARF6\text{-}GDP}$ cells that were capable of colonizing at secondary sites had overcome the inhibitory effects of mutant ARF6 on ERK activation. Given this finding, ERK activity was also examined in $LOX^{ARF6\text{-}GDP}$ primary tumors. We found that the level of phospho-ERK was dependent on tumor size, as $LOX^{ARF6\text{-}GDP}$ cells cultured from larger tumors exhibited higher phospho-ERK levels compared with cells derived from the smallest tumor or the parental cell line (Fig. 5*D*). Thus, compensatory mechanisms are in place to rescue ERK signaling in $LOX^{ARF6\text{-}GDP}$ cells *in vivo*. ERK levels stayed relatively constant in cell lines subcultured from the $LOX^{ARF6\text{-}GTP}$ and LOX^{GFP} primary tumors (data not shown).

Phospholipase D (PLD) activity is elevated in a large variety of cancers (20, 21). PLD also promotes ERK activation by increasing the membrane-associated pool of phosphorylated Raf (22, 23). ARF6 activates PLD and a role for PLD has been described in ARF6-regulated endosome recycling, epithelial cell migration, and regulated secretion (5). We hypothesized that ARF6 promotes ERK phosphorylation during cell invasion by activating PLD activity. Indeed, we find that phospho-ERK levels in LOX^{GFP} and $LOX^{ARF6\text{-}GTP}$ cells subcultured from the primary tumor are decreased upon treatment with primary alcohols such as 1-butanol that interrupts PLD catalyzed formation of phosphatidic acid (PA). Treatment with 4-butanol was used as a control (Fig. 6*A*). Next, we investigated PLD activity in $LOX^{ARF6\text{-}GDP}$ subcultures from sites of metastases relative to original $LOX^{ARF6\text{-}GDP}$ cell line by examining the accumulation of PA using a fluorescent probe, GFP-PA binding domain (GFP-PA binding domain of SNAP 25), shown to function as a specific sensor of PA (9). As seen in Fig. 6*B*, PLD activity was significantly higher in $LOX^{ARF6\text{-}GDP}$ cells subcultured cells, suggesting that in the absence of ARF6 activation, other signals ensue *in vivo* to elevate PLD activity. Inhibition of PLD activity, as described above, blocked ERK phosphorylation in these subcul-tured cells (Supplementary Fig. S5*A*). PLD inhibition also blocked invadopodia formation and cell invasion in $LOX^{ARF6\text{-}GDP}$ cells subcultured cells *in vitro* assays (Supplementary Fig. S5*B* and *C*).

How does ERK activation downstream of ARF6 promote cell invasion? We examined Rac1 activation in LOX, $LOX^{ARF6\text{-}GTP}$ cell lines, and invasive subcultured $LOX^{ARF6\text{-}GDP}$ cells because (a) Rac1 activation downstream of ERK has been shown to have a role in cell invasion (24) and (*b*) Rac1 activation downstream of ARF6 has been shown to regulate cell motility (5). We show that Rac1-GTP levels are increased in $LOX^{ARF6\text{-}GTP}$ cells and subcultured $LOX^{ARF6\text{-}GDP}$ cells relative to basal Rac1-GTP in LOX cell lines (Fig. 6*C*). In all three cell lines, Rac1 activation was abolished by treatment with MAP/ERK kinase inhibitors, suggesting that Rac1 activation occurs downstream of ERK (data not shown). In *in vitro* cell invasion assays, expression of dominant-negative Rac1 blocked basal as well as ARF6-GTP induced cell invasion (Fig. 6*D*). Taken together these studies suggest that ARF6→PLD→ERK→Rac1 module regulates the process of tumor cell invasion.

Discussion

Here, we report on the results of an *in vivo* study in which the effects of perturbing the ARF6 GTP/GDP cycle on the tumorigenic and metastatic progression of melanoma was examined. We used a well-characterized mouse model to investigate the effect of ARF6

mutants on subcutaneous melanoma tumor growth and lung metastasis. Sustained activation of ARF6 through the expression of an ARF6-GTP mutant hampered growth of the primary tumor but augmented the invasive potential of LOX cells in the primary tumor. The expression of dominant-negative ARF6, ARF6(T27N), slowed down the growth rate of the primary tumor mass and by and large showed a reduction in the degree of primary tumor cell invasion into the surrounding tissue. Furthermore, lungs excised from mice injected i.v. with $LOX^{ARF6\text{-}GDP}$ cells displayed a lower incidence of lung metastasis and less tumor burden compared with lungs of control animals. This work is consistent with our previous work wherein the effects of GTP/GDP cycling ARF6 mutants were examined in LOX cells using *in vitro* cell invasion assay.

The constitutive activation of ARF6 enhances invasive capacity via ERK activation (6). We show that ERK signaling in ARF6 tumors is dependent on PLD activation. The current study also suggests that compensatory mechanisms are in place that rescue deficient PLD and ERK signaling in the $LOX^{ARF6\text{-}GDP}$ cells *in vivo*, as cells cultured from $LOX^{ARF6\text{-}GDP}$ primary or lung tumor explants exhibited higher phospho-ERK levels compared with the parental cells. How might ARF6-PLD-ERK signaling promote cell invasion? Our previous studies have shown that ARF6 activation increases the rate of invadopodia turnover, making cells more invasive (6). Indeed, inhibition of PLD and ERK blocks invadopodia formation in cells isolated from LOX and $LOX^{ARF6\text{-}GTP}$ tumors. Furthermore, cells derived from $LOX^{ARF6\text{-}GDP}$ tumor explants regain the ability to form invadopodia. The studies shown here also indicate that ERK activation leads to increased Rac1-GTP levels and invadopodia formation is dependent on Rac1 activation downstream of ERK activation. Rac1 activation in turn could promote actin remodeling required for invadopodia extension or facilitate the recruitment of actinbinding proteins as has been described (17) In addition to its control of invadopodia formation, ARF6 might also regulate the trafficking/ release of proteases such as the membrane type metalloproteases (25) at the invasive front.

The slow growth rate of $LOX^{ARF6\text{-}GTP}$ tumors correlated with a reduced proliferation rate *in vitro*. A low level of Myc expression, a marker for cell proliferation, in $LOX^{ARF6\text{-}GTP}$ cells relative to parental LOX cells, also correlates with reduced cell proliferation. These findings are in alignment with previous reports by us and others that the efficiency of completion of cytokinesis is significantly reduced upon sustained activation of ARF6 (26–28). As described here, sustained ARF6 activation leads to an increase in primary tumor cells at the G_2-M stage of the cell cycle. At this time, we cannot exclude a direct role for ARF6 in other cell proliferation signaling responses that may also account for the dramatic decrease in proliferation rate observed in $LOX^{ARF6\text{-}GTP}$ tumors. The dramatic effect of active ARF6 on cell proliferation was evident also in the development of metastatic foci in the lungs. Typically individual tumor cells proliferate to form microscopic nodules that eventually form macrometastatic lesions. $LOX^{ARF6\text{-}GTP}$ cells did not lead to any visible macroscopic lesions in the lung as opposed to LOX^{GFP} cells where macroscopic lesions were clearly evident. Lesions were also observed in animals injected with $LOX^{ARF6\text{-}GDP}$ cells, although these were smaller and of lower incidence relative to control animals. These studies suggest that ARF6 cycling may be required for the development of macrometastases at distal sites.

Whether there is a direct correlation between tumor size and disease prognosis is still ambiguous, although studies have indicated that the probability of developing metastases increases with tumor size (29). Of important note however is that the ARF6-GTP tumors despite their small size are significantly more invasive than their parental counterparts. Similar opposing effects on tumor size and invasion capacity have been reported in skin carcinogenesis models of p53 and Tiam 1–deficient mice (30, 31). These apparently opposing effects of ARF6 activation on tumor cell proliferation and invasion may indeed be

a reflection of a requirement for ARF6 cycling, and that its altered regulation could have varying outcomes during the different stages of tumor progression.

Given the functions of ARF6 in many cellular processes and pathways, our results support accumulating evidence that ARF6 coordinates mechanisms underlying tumor cell proliferation, motility, and invasion—all of which are crucial for tumor growth, maintenance, and metastasis. These findings have widespread implications for the function of ARF6 as a potent regulator of tumor growth and metastatic behavior *in vivo*.

Supplementary Material

Refer to Web version on PubMed Central for supplementary material.

Acknowledgments

Grant support: A subproject of a Program Project Grant to the Notre Dame-Walther Cancer Center from the Department of Defense, U.S. Army Medical Research, and Materiel Command (C.D. Souza-Schorey and J. Schorey), and by a grant from the NIH (CA115316-01; C.D. Souza-Schorey).

We thank Dr. Felipe Palacios for the pTRE2:ARF6 mutant plasmids, Dr. Julia Knight (Mathematics, Notre Dame) for invaluable assistance with doubling time measurements, Linda Van Aelst and Philippe Chavrier for helpful comments, and Kandus Kruger-Passig and Mayra Sandoval-Cooper for excellent technical assistance.

References

1. Hanahan D, Weinberg RA. The hallmarks of cancer. Cell. 2000; 100:57–70. [PubMed: 10647931]
2. Chen WT, Wang JY. Specialized surface protrusions of invasive cells, invadopodia and lamellipodia, have differential MT1-MMP, MMP-2, and TIMP-2 localization. Ann N Y Acad Sci. 1999; 878:361–371. [PubMed: 10415741]
3. Monsky WL, Lin CY, Aoyama A, et al. A potential marker protease of invasiveness, seprase, is localized on invadopodia of human malignant melanoma cells. Cancer Res. 1994; 54:5702–5710. [PubMed: 7923219]
4. Donaldson JG. Multiple roles for Arf6: sorting, structuring, and signaling at the plasma membrane. J Biol Chem. 2003; 278:41573–41576. [PubMed: 12912991]
5. D'Souza-Schorey C, Chavrier P. ARF proteins: roles in membrane traffic and beyond. Nat Rev Mol Cell Biol. 2006; 7:347–358. [PubMed: 16633337]
6. Tague SE, Muralidharan V, D'Souza-Schorey C. ADP-ribosylation factor 6 regulates tumor cell invasion through the activation of the MEK/ERK signaling pathway. Proc Natl Acad Sci U S A. 2004; 101:9671–9676. [PubMed: 15210957]
7. Hashimoto S, Onodera Y, Hashimoto A, et al. Requirement for Arf6 in breast cancer invasive activities. Proc Natl Acad Sci U S A. 2004; 101:6647–6652. [PubMed: 15087504]
8. Li M, Ng SS, Wang J, et al. EFA6A enhances glioma cell invasion through ADP ribosylation factor 6/ extracellular signal-regulated kinase signaling. Cancer Res. 2006; 66:1583–1590. [PubMed: 16452216]
9. Zeniou-Meyer M, Zabari N, Ashery U, et al. Phospholipase D1 production of phosphatidic acid at the plasma membrane promotes exocytosis of large dense-core granules at a late stage. J Biol Chem. 2007; 282:21746–21757. [PubMed: 17540765]
10. Boshans RL, Szanto S, van Aelst L, et al. ADP-ribosylation factor 6 regulates actin cytoskeleton remodeling in coordination with Rac1 and RhoA. Mol Cell Biol. 2000; 20:3685–3694. [PubMed: 10779358]
11. Hoover H, Muralidharan-Chari V, Tague S, et al. Investigating the role of ADP-ribosylation factor 6 in tumor cell invasion and extracellular signal-regulated kinase activation. Methods Enzymol. 2005; 404:134–147. [PubMed: 16413265]
12. Cirri P, Taddei ML, Chiarugi P, et al. Insulin inhibits platelet-derived growth factor-induced cell proliferation. Mol Biol Cell. 2005; 16:73–83. [PubMed: 15525682]

13. Whiteland JL, Nicholls SM, Shimeld C, et al. Immunohistochemical Detection of T-cell subsets and other leukocytes in paraffin-embedded Rat and Mouse tissues with monoclonal antibodies. J Histochem Cytochem. 1995; 43:313–320. [PubMed: 7868861]
14. Webb CP, Van Aelst L, Wigler MH, et al. Signaling pathways in Ras-mediated tumorigenicity and metastasis. Proc Natl Acad Sci U S A. 1998; 95:8773–8778. [PubMed: 9671754]
15. Schweitzer JK, D'Souza-Schorey C. Localization and activation of the ARF6 GTPase during cleavage furrow ingression and cytokinesis. J Biol Chem. 2002; 277:27210–27216. [PubMed: 12016212]
16. Arvanitis C, Felsher DW. Conditionally MYC: insights from novel transgenic models. Cancer Lett. 2005; 226:95–99. [PubMed: 16039948]
17. Weed SA, Du Y, Parsons JT. Translocation of cortactin to the cell periphery is mediated by the small GTPase Rac1. J Cell Sci. 1998; 111:2433–2443. [PubMed: 9683637]
18. Kjonniksen I, Storeng R, Pihl A, et al. A human tumor lung metastasis model in athymic nude rats. Cancer Res. 1989; 49:5148–5152. [PubMed: 2766284]
19. Yang M, Jiang P, An Z, et al. Genetically fluorescent melanoma bone and organ metastasis models. Clin Cancer Res. 1999; 5:3549–3559. [PubMed: 10589771]
20. Rodrik V, Gomes E, Hui L, et al. Myc stabilization in response to estrogen and phospholipase D in MCF-7 breast cancer cells. FEBS Lett. 2006; 580:5647–5652. [PubMed: 16996503]
21. Zheng Y, Rodrik V, Toschi A, et al. Phospholipase D couples survival and migration signals in stress response of human cancer cells. J Biol Chem. 2006; 281:15862–15868. [PubMed: 16595654]
22. Andresen BT, Rizzo MA, Shome K, et al. The role of phosphatidic acid in the regulation of the Ras/MEK/ Erk signaling cascade. FEBS Lett. 2002; 531:65–68. [PubMed: 12401205]
23. Hong JH, Oh SO, Lee M, et al. Enhancement of lysophosphatidic acid-induced ERK phosphorylation by phospholipase D1 via the formation of phospha-tidic acid. Biochem Biophys Res Commun. 2001; 281:1337–1342. [PubMed: 11243883]
24. Vial E, Sahai E, Marshall CJ. ERK-MAPK signaling coordinately regulates activity of Rac1 and RhoA for tumor cell motility. Cancer Cell. 2003; 4:67–79. [PubMed: 12892714]
25. Osenkowski P, Toth M, Fridman R. Processing, shedding, and endocytosis of membrane type 1-matrix metalloproteinase (MT1-MMP). J Cell Physiol. 2004; 200:2–10. [PubMed: 15137052]
26. Dyer N, Rebollo E, Dominguez P, et al. Spermatocyte cytokinesis requires rapid membrane addition mediated by ARF6 on central spindle recycling endosomes. Development. 2007; 134:4437–4447. [PubMed: 18039970]
27. Schweitzer JK, D'Souza-Schorey C. A requirement for ARF6 during the completion of cytokinesis. Exp Cell Res. 2005; 311:74–83. [PubMed: 16181626]
28. Fielding AB, Schonteich E, Matheson J, et al. Rab11-3 and FIP4 interact with Arf6 and the exocyst to control membrane traffic in cytokinesis. EMBO J. 2005; 24:3389–3399. [PubMed: 16148947]
29. Heimann R, Hellman S. Aging, progression, and phenotype in breast cancer. J Clin Oncol. 1998; 16:2686–2692. [PubMed: 9704718]
30. Kemp CJ, Donehower LA, Bradley A, et al. Reduction of p53 gene dosage does not increase initiation or promotion but enhances malignant progression of chemically induced skin tumors. Cell. 1993; 74:813–822. [PubMed: 8374952]
31. Malliri A, van der Kammen RA, Clark K, et al. Mice deficient in the Rac activator Tiam1 are resistant to Ras-induced skin tumours. Nature. 2002; 417:867–871. [PubMed: 12075356]

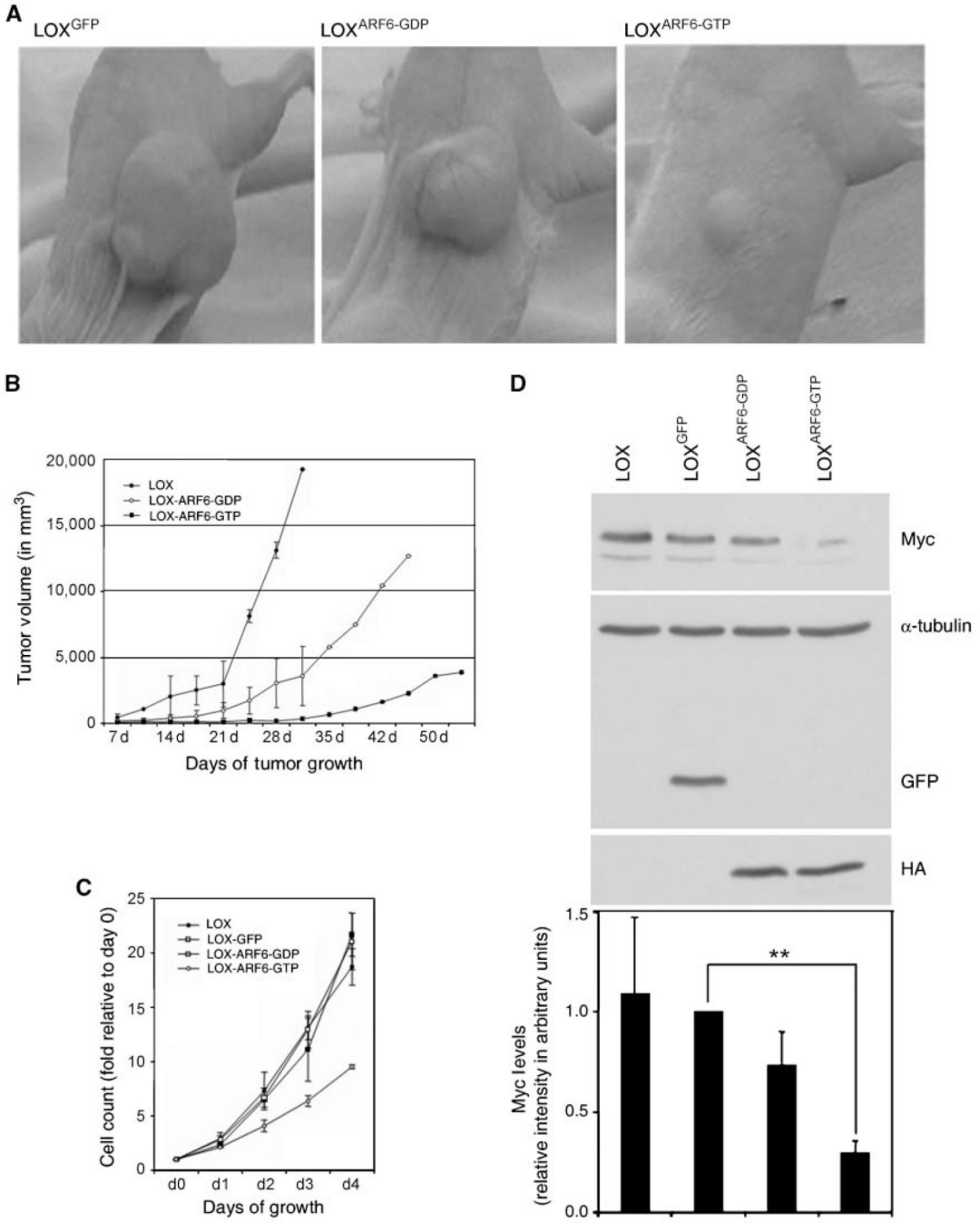

Figure 1.

Growth characteristics of primary LOX tumors and LOX cell lines. *A* and *B*, mice were injected s.c. with LOX^{GFP}, $LOX^{ARF6\text{-}GDP}$, or $LOX^{ARF6\text{-}GTP}$ cells in the dorsal flank. Photographs of representative tumors at 3 wk postinjection are shown. Progression of tumor volumes at the indicated days postinjection is plotted. *C*, 2.5×10^4 LOX^{GFP}, $LOX^{ARF6\text{-}GDP}$, and $LOX^{ARF6\text{-}GTP}$ cells were plated in triplicate, stained with crystal violet, and the proliferation rates are shown as an average of two independent experiments. *D*, lysates from respective cell lines were subjected to SDS-PAGE and probed with Myc, HA, GFP, and α-tubulin (loading control) antibodies. A representative blot is shown. The graph

displays the densitometric intensity of the Myc band from three independent experiments. *Columns*, mean; *bars*, SD; **, $P < 0.002$.

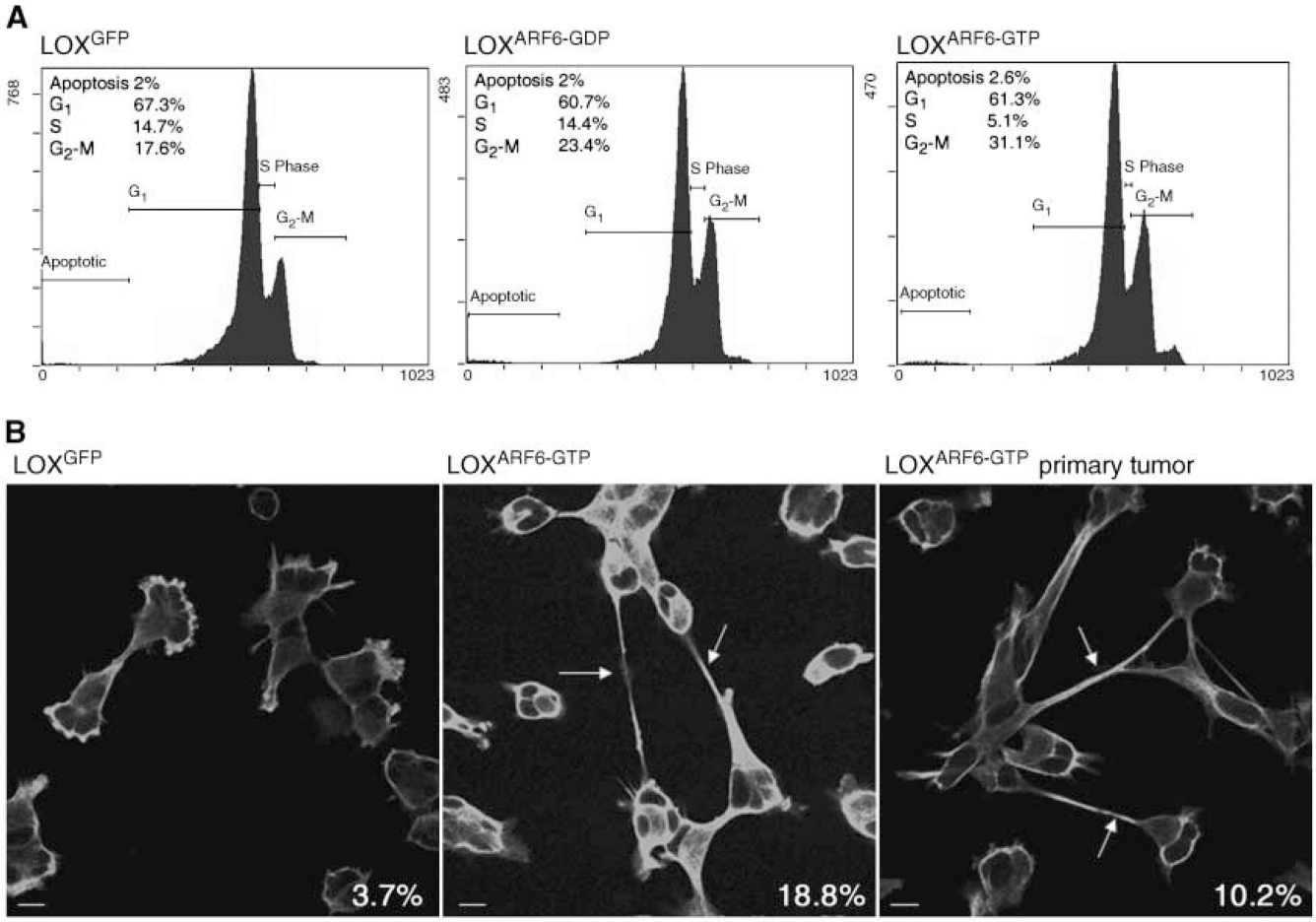

Figure 2.

Characterization of cell cycle progression. *A*, LOX^{GFP}, LOX$^{ARF6\text{-}GDP}$, or LOX$^{ARF6\text{-}GTP}$ cells were subjected to cell cycle analysis as described. The percentage of cells in each phase of the cell cycle is shown. *B*, LOX^{GFP}, LOX$^{ARF6\text{-}GTP}$ cell lines, and subcultured cells from the LOX$^{ARF6\text{-}GTP}$ primary tumor were synchronized at G_2-M, and progression through mitosis was monitored. Cells were fixed and stained for α-tubulin at 5 h post entry into mitosis. The percentage of cells exhibiting tubulin-positive intercellular bridges (*arrows*) is indicated on the bottom right of each image.

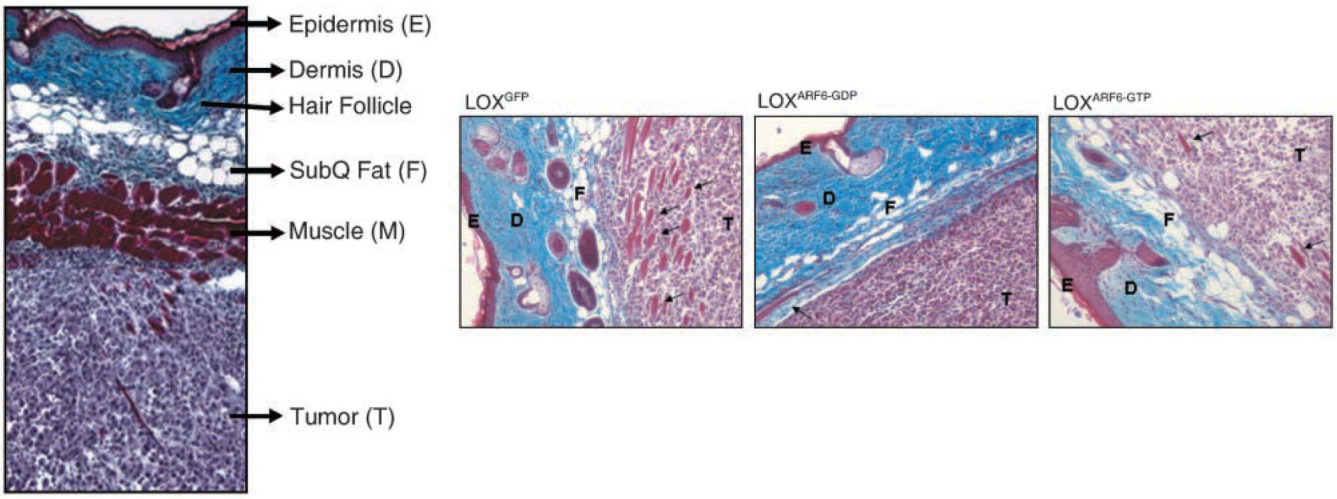

Figure 3.

Morphologic analysis of time-matched LOX^{GFP}, $LOX^{ARF6\text{-}GTP}$, and $LOX^{ARF6\text{-}GDP}$ tumors. *Left*, representative cross-section through intact skin, 2 wk post s.c. injection of LOX cells. The epidermis, dermis, subcutaneous fat (*subQ fat*), and muscle is intact. The tumor with intact collagen border is below the muscle layer. *Right*, histologic sections of primary tumors and surrounding tissues at 3 wk post injection of tumor cell lines. Note the compromise of fat and muscle layers (*arrows*), which is maximal in $LOX^{ARF6\text{-}GTP}$ tumors and less in $LOX^{ARF6\text{-}GDP}$ tumors relative to parental LOX tumors. Sections were stained with Masson's Trichrome (*black*, nuclei; *red*, muscle; *blue*, collagen).

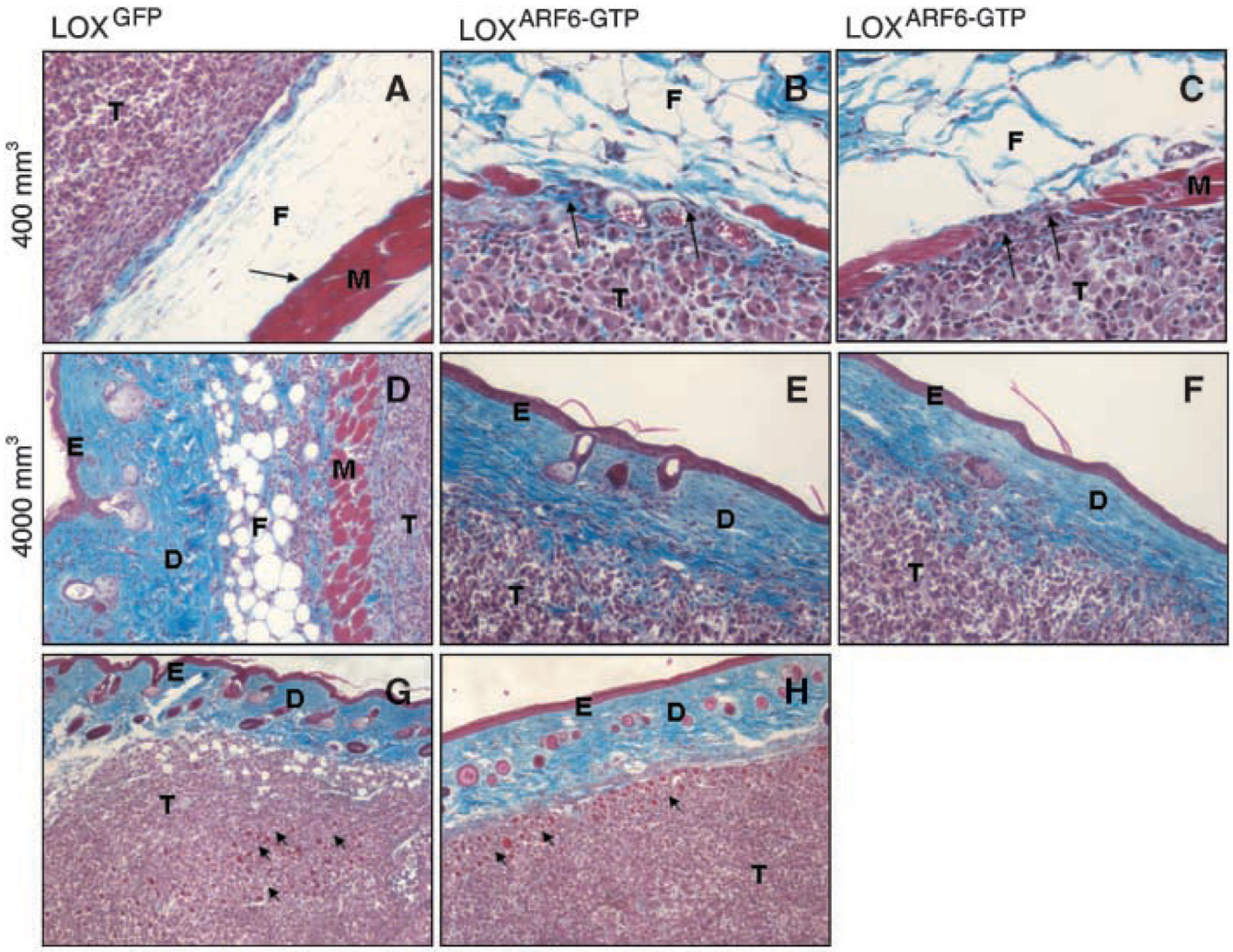

Figure 4.

$LOX^{ARF6\text{-}GTP}$ tumors are highly invasive. *A* to *C*, LOX^{GFP} (*A*), $LOX^{ARF6\text{-}GTP}$ (*B* and *C*) tumors of size ~400 mm^3 were fixed, processed for histology, and stained with Masson's Trichrome. The tumor border of LOX-GFP cells is intact whereas $LOX^{ARF6\text{-}GTP}$ tumors exhibit areas of invasion at tumor-muscle border. *Arrows*, muscle fibers, which are intact in *A* but compromised in *B* and *C*. *D* to *F*, LOX^{GFP} (*D*) and $LOX^{ARF6\text{-}GTP}$ (*E* and *F*) tumors of ~4,000 mm^3 size were examined by histologic analysis. Representative images of $LOX^{ARF6\text{-}GTP}$ tumor cells in *E* and *F* invading far into the epidermis are shown. Muscle fibers and fat tissue are fully comprised in these tissues. *G* and *H*, sections of LOX^{GFP} (19,253 mm^3; *G*) and $LOX^{ARF6\text{-}GTP}$ (5,045 mm^3; *H*) tumors exhibiting a similar degree of invasion at the tumor border interface. Arrows indicate the muscle layer and show similar skin tissue compromise, although the parental LOX tumor is much larger. *T*, tumor; *F*, fat; *M*, muscle; *E*, epidermis; *D*, dermis.

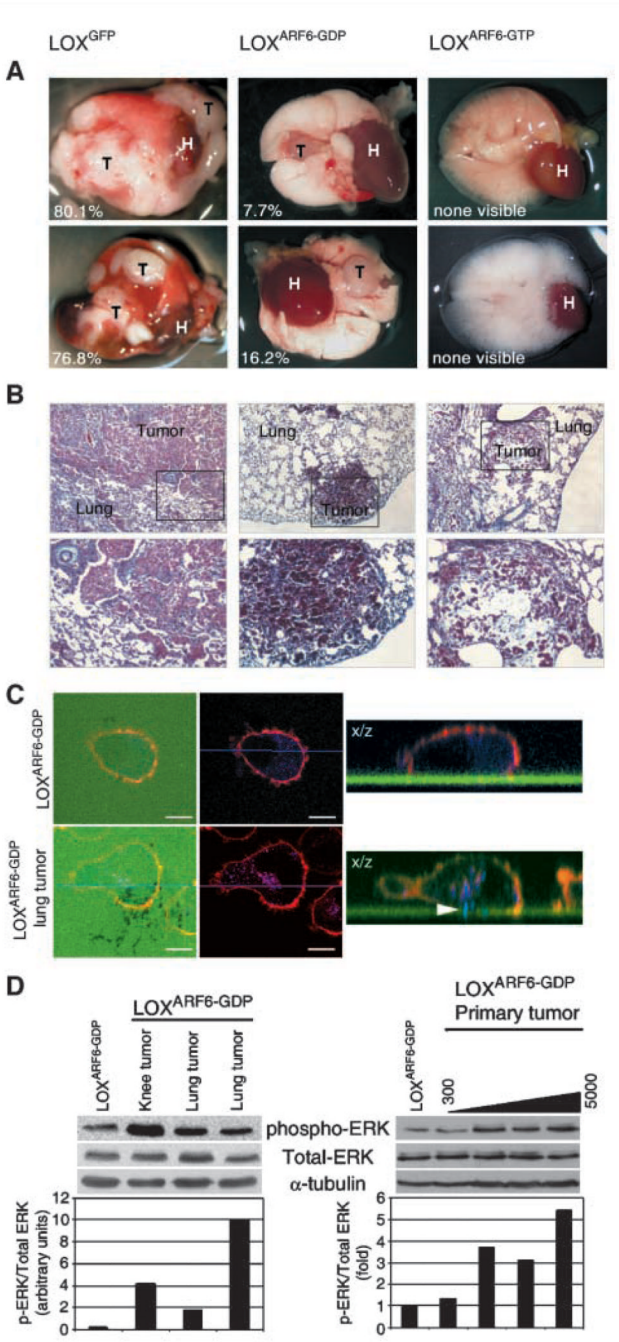

Figure 5.

Experimental metastasis of LOX$^{ARF6\text{-}GTP}$ and LOX$^{ARF6\text{-}GDP}$ cells. *A*, photographs of whole lungs from representative LOX^{GFP}, LOX$^{ARF6\text{-}GDP}$, or LOX$^{ARF6\text{-}GTP}$ mice post tail vein injection at 43, 53, and at 61 d, respectively. The lungs of mice injected with LOX^{GFP} showed the greatest extent of macrometastatic lesions in each lobe. LOX$^{ARF6\text{-}GDP}$-injected mice exhibited fewer and smaller macrometastatic lesions. No visible metastasic lesions were seen in LOX$^{ARF6\text{-}GTP}$-injected mice. The percentage of tumor tissue to total lung tissue is indicated. *H*, heart; *T*, tumor. *B*, histologic analysis of lungs from experimental metastasis assays. *Top* and *bottom*, representative sections from LOX^{GFP} LOX$^{ARF6\text{-}GTP}$, and LOX$^{ARF6\text{-}GDP}$ lung tumors at x10 and x20 magnification, respectively. All lungs were

time matched at 53 d post tail-vein injection. *C*, characterization of invasiveness in $LOX^{ARF6\text{-}GDP}$ and subcultured LOXARF6-GDP cells Parental LOXARF6-GDP and subcultured LOXARF6-GDP cells from lung tumors were plated on FITC-gelatin-coated coverslips (*green*) and allowed to invade (*top* and *bottom*, respectively). Cells were fixed and stained for actin (*red*) and cortactin (*blue*) and imaged using confocal microscopy. *Arrowhead*, protruding invadopodia. *D*, ERK activation in invasive $LOX^{ARF6\text{-}GDP}$ cells. Lysates were prepared from parental $LOX^{ARF6\text{-}GDP}$ cells and from cells subcultured from metastatic tumors (*left*) or from primary tumors ranging from 300 to 5,000 mm^3 in size (*right*) and subjected to Western Blot analysis. Blots were probed for phospho-ERK, total ERK, and a-tubulin (loading control). Band density was measured by densitometry, and the ratios of ERK to phospho-ERK is shown. A representative blot of three separate experiments is shown.

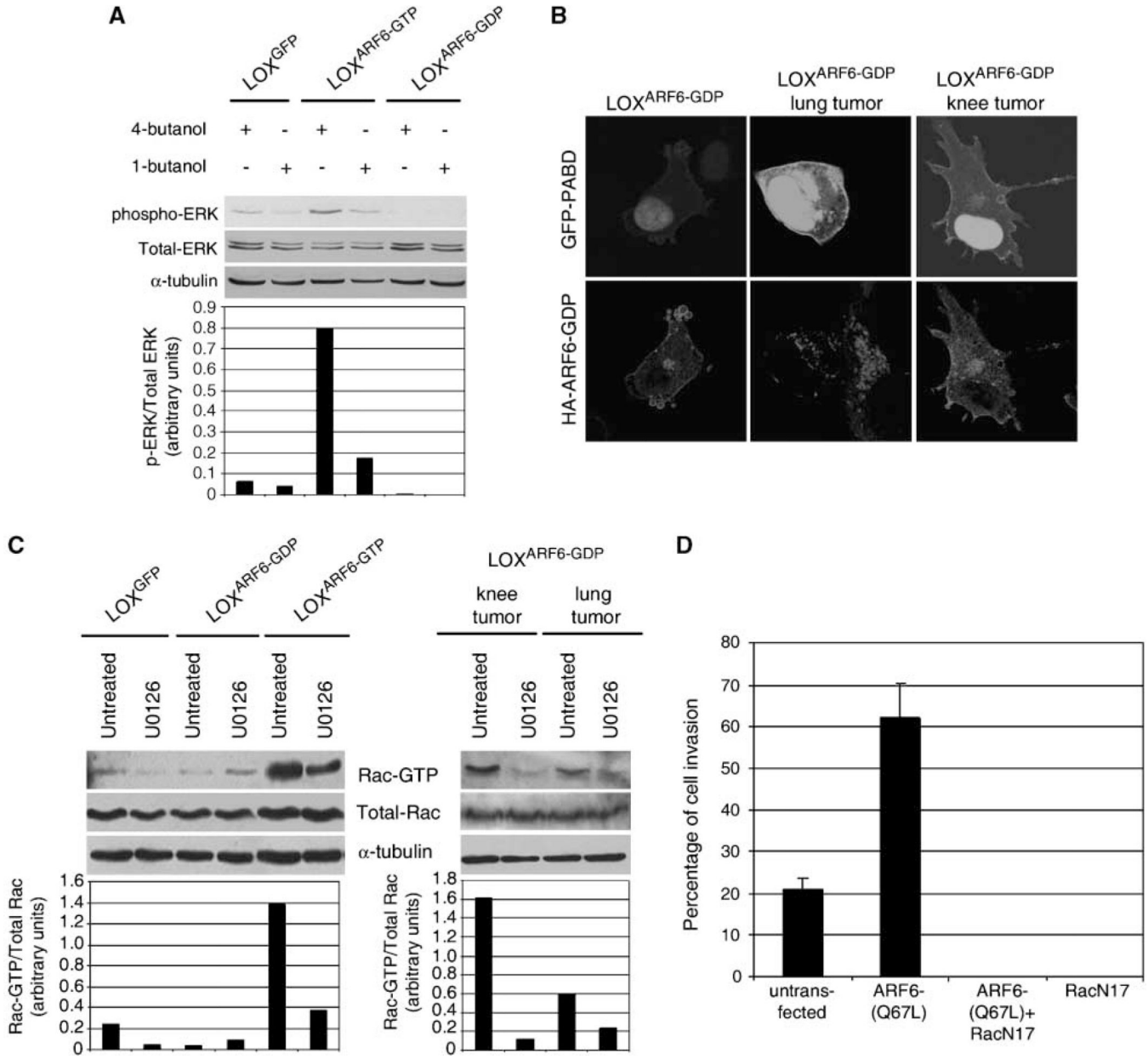

Figure 6.

PLD activity is required for ERK activation, and Rac1 activation downstream of ERK is required for cell invasion. *A*, LOX^{GFP}, $LOX^{ARF6\text{-}GDP}$, and $LOX^{ARF6\text{-}GTP}$ cells were treated with 0.3% of 4-butanol or 1-butanol as indicated. Cell lysates were probed for phospho-ERK or total ERK by Western blotting. The blots were reprobed with α-tubulin as a loading control. Band density was measured by densitometry, and the ratios of ERK to phospho-ERK is shown. *B*, images of $LOX^{ARF6\text{-}GDP}$ and subcultured $LOX^{ARF6\text{-}GDP}$ cells from metastatic tumor explants expressing GFP-PA binding domain (*green*), and stained with HA antibody to detect ARF6-GDP, are shown. Identical acquisition settings were used to image GFP-PA binding domain in each sample. *C*, Rac1 activation occurs downstream of ERK signaling during cell invasion. LOX^{GFP}, $LOX^{ARF6\text{-}GDP}$, and $LOX^{ARF6\text{-}GTP}$ cell lines and $LOX^{ARF6\text{-}GDP}$ cells from metastasized tumors were seeded on gelatin-coated coverslips and allowed to invade in the presence or absence of 20 μmol/L U0126. Lysates of cells for each

condition were then subjected to the PAK-binding assay and immunoblotted for Rac1. Cell lysates were also probed for total Rac1 and for α-tubulin (loading control). Band density was measured by densitometry, and the ratio of Rac1-GTP to total Rac1 is shown. *D*, inactivation of Rac1 inhibits basal and ARF6-GTP–induced invasion. LOX cells were transiently transfected with plasmid expressing Rac1(T17N) alone or with an expression plasmid for HA-ARF6(Q67L) and seeded on FITC-gelatin–coated coverslips. Cells were fixed and labeled for Rac1 or for Rac1 and HA. Cells expressing with Rac1(T17N) alone or coexpressing Rac1(T17N) and ARF6(Q67L) and exhibiting matrix degradation underneath were scored and the percentage of invasion is shown.